Metallization of nanobiostructures: a theoretical study of copper nanowires growth in microtubules

Bartosz Trzaskowski,*[a] Pierre A. Deymier[b] and Ludwik Adamowicz[a]

Received 28th July 2006, Accepted 26th September 2006
First published as an Advance Article on the web 12th October 2006
DOI: 10.1039/b610844j

A theoretical study of possible metallization sites within polypeptide structures is reported. The study has involved performing density functional B3LYP calculations in order to describe the affinities of various amino acids and larger peptide fragments towards copper ions. The results obtained for small amino acid systems have been used in the theoretical analysis of feasible metallization sites in large protein segments and in the whole proteins. The goal of this study was to explain the preferred inner-surface copper metallization of microtubules over outer-surface metallization. The inner-surface metallization is a new process that yields copper wires of 15 nm in diameter and may be used for fabrication of molecular interconnects at the nano-device level.

Introduction

Nowadays, one of the most important challenges for the semiconductor industry is to design and manufacture nano-sized electronic circuits. The traditional semiconductor technology and the top-down lithography approach of fabricating electronic devices with increasingly smaller dimensions becomes expensive and slowly reaches its limits. In view of this, it has been proposed that new, bottom-up manufacturing techniques should be developed and replace the traditional approaches.[1–4] The new techniques must rely on the development of a new technology for manufacturing nano-interconnects that may utilize molecular or biomolecular systems as templates.

Already several biological systems have been proposed as good candidates for nanosized templates for interconnectors. Most studies in this area have been performed on DNA molecules. It has been shown that DNA may be used as a template to form silver nanowires connecting gold electrodes.[5] DNA has also been metallized using palladium,[6,7] platinum,[8,9] gold,[10,11] copper,[12,13] and cobalt[14] to yield stable nanosized wires. Others have used different native biological and biologically-inspired templates, such as viruses,[15,16] peptides,[17] and peptide nanotubes,[18] in nano-wire production. All these approaches have focused on one-dimensional nanowires, which may be important elements for the manufacturing of nanoscale electronic circuits and devices.

Microtubules (MTs) comprise another interesting type of system that may be a good candidate for designing and manufacturing electronic nanodevices. MTs are filamentous intracellular structures responsible for various types of movements in eukaryotic cells. They form long (0.2–20 μm) cylindrical structures that are 25 nm in diameter with a 15 nm hollow core and are composed of 13 protofilaments. The building blocks of protofilaments are tubulin dimers composed of α- and β-tubulins. The structures of microtubules[19] and the α–β tubulin dimer[20,21] have been recently described using cryo-electron microscopy and crystallography.

The polarity of microtubules[22,23] and their naturally high chemical specificity inherent in the different natures of their two ends provide a means of directing and controlling their attachment to surfaces.[24–26] Also, immobilization of MTs on surfaces and their subsequent metallization offers a number of possible chemical and biological applications of these systems. Early experiments on utilizing the MTs had shown that these biological structures may be efficiently metallized by Ni or Co to yield nanowires with diameters of 50 nm.[27,28] Recently, a new method of microtubule metallization by Cu has been introduced.[29] In the experiments involving that method, the MT metallization generated long (several micrometers) copper nanowires, with diameters equal to the inner diameter of the nanotube (15 nm). The selective metallization of the inner MT surface was achieved by a biologically-benign electroless deposition process with ascorbic acid as the redox reagent.

In this work we present a theoretical study of the selective metallization of biomacromolecules. We use the density functional B3LYP theory to describe the affinities of amino acids towards Cu^{2+} ions and to build a database on the amino acid–copper interactions. To account for the structural flexibility of the protein fragments and to describe how this effect influences the affinities, we have also calculated affinities for selected peptides. In addition, we have characterized the interactions between copper ions and fragments of MTs to find the most probable metallization sites. This theoretical study allows us to elucidate the mechanism of selective MT metallization.

Models and computational details

In this work we have used three different levels of theory to describe the process of MT metallization by copper ions. In the first part of the study we have focused on copper–amino acids

[a]*Department of Chemistry, University of Arizona, Tucson, Arizona, 85721, USA. E-mail: trzask@u.arizona.edu; Fax: +1 520 6218407; Tel: +1 520 6216761*
[b]*Department of Materials Science & Engineering, University of Arizona, Tucson, Arizona, 85721, USA. E-mail: deymier@email.arizona.edu; Tel: +1 520 6216080*

This journal is © The Royal Society of Chemistry 2006

affinities. To save computational effort we have used simplified molecular models of amino acids that only include the most important fragments of the amino acid molecules from the viewpoint of the interactions with Cu^{2+}. Such simplified models are commonly used in computational studies and, if the models are chosen correctly, the simplifications usually have little effect on the results of the calculations.[30,31] In this study we have constructed models of all the amino acids that have high affinity towards the Cu^{2+} ion, *i.e.* arginine, asparagine, aspartate, cysteine, cystine, glutamine, glutamate, histidine, lysine, methionine, proline, selenocysteine, serine, threonine, tryptophan, and tyrosine (depicted in Fig. 1). Additionally we have performed calculations for some model peptides and on the N-terminus of the protein. To validate the models we have also performed calculations for selected amino acids (cysteine, glutamate, histidine, lysine, serine) without simplifying the structures. We have found out that the energies obtained using simplified and non-simplified models were identical within 2 kcal/mol, well below the average error of the B3LYP method for the transtion metals system.[32]

In the second part of this work we have focused on steric and geometrical features of small peptides and how they affect the Cu^{2+} ion binding. For this part of the study we have chosen a tripeptide His-Val-His as a model. This model was chosen because it has been used before and because it was very well described using several experimental techniques.[33]

The last part of this work is devoted to copper metallization of the entire protein. We have used the MT as a model protein in the study. Owing to limited computational resources, the size of the model had to be relatively small and, thus, we have used the approach employed before in computational studies of enzymatic reaction mechanisms where similar size limitations also appeared.[30,31,34] First, all possible metallization sites in the MT were examined using the results described in the previous sections. Next, relatively small models of all the metallization sites were constructed. All the models contained the full-atom model of the amino acid with the high affinity towards copper, as well as full-atom models of all neighboring amino acid residues located not further than 3.0 Å from the metallization center. This yielded models containing 40–80 atoms.

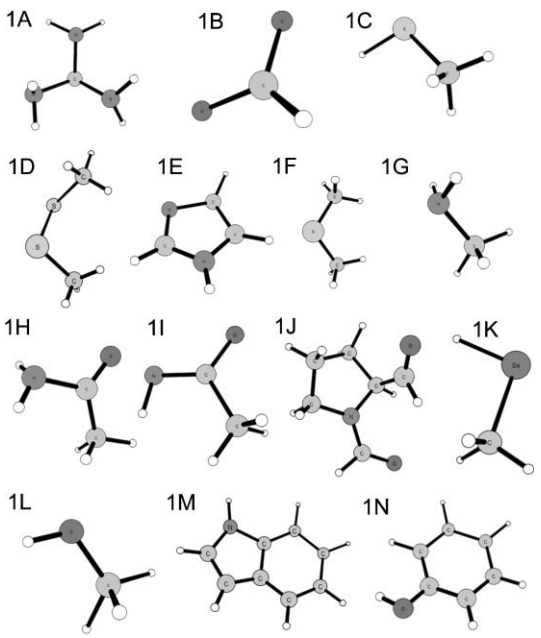

Fig. 1 Molecular models of amino acids and peptide fragments used in this work: 1A arginine; 1B aspartate, glutamate or C-terminus of a protein; 1C cysteine; 1D cystine; 1E histidine; 1F methionine; 1G lysine or N-terminus of a protein; 1H asparagine, glutamine or peptide bond; 1I deprotonated peptide bond; 1J proline; 1K selenocysteine; 1L serine or threonine; 1M tryptophan; 1N tyrosine.

All calculations were performed using the density functional B3LYP method[35,36] with the standard 6-31G* basis set. The preliminary optimizations of the protein-fragment models were performed using the molecular mechanics method with the amber96 force-field[37] and using the semiempirical PM3 method.[38] Calculations have been done for the isolated systems and for the systems immersed in water. The solvation was described using the polarizable continuum model (PCM).[39] For the molecular models of the amino acids and the peptides, full optimization of all geometrical parameters was performed. In the geometry optimization of the protein, the coordinates of its backbone atoms were kept frozen to account for the limited movement of the amino acid residues resulting from the rigid 3D arrangement of the structure of the whole protein.[30,31,34,40] In all calculations concerning the isolated and hydrated molecular models of the amino acids and the peptides, Hessian matrices were calculated in order to assess whether the predicted equilibrium geometries corresponded to true energy minima. The zero-point energy corrections, scaled by a factor of 0.96, were added to the final energies.[41] The calculations were performed using the quantum chemistry package Gaussian 03.[42]

Results and discussion

Cu^{2+}–amino acid affinity

The binding of Cu^{2+} to histidine and other amino acids was first studied in the early 1970s[43,44] after the discovery that many Cu-containing enzymes may have superoxide dismutase activity.[45,46] Since then, a large number of experimental studies have been performed concerning the Cu^{2+}–amino acid interactions, and different aspects of the copper affinity toward amino acids have been analyzed.[47–53] In most of these studies, however, the authors concentrated solely on the histidine–Cu^{2+} system due to its importance in various applications. Studies on other amino acids have been scarce. To fill this void, we have undertaken a comprehensive investigation of the affinity of the copper(II) ion towards all amino acids and protein fragments that have at least one heteroatom. To quantify the affinity of the metal ion towards amino acids, we have considered the following model reaction:

$$[Cu(H_2O)_4]^{2+} + aa \rightarrow [Cu(H_2O)_3(aa)]^{2+} + H_2O \qquad (1)$$

where "aa" stands for the amino acid. Reaction (1) allows us to determine the relative affinity corresponding to the Cu^{2+}–aa system with respect to the affinity of copper(II) to water.

The results obtained in the calculations and summarized in Table 1 suggest that a model that does not include the presence

 This journal is © The Royal Society of Chemistry 2006

Table 1 Theoretical values of relative Cu^{2+}–amino acid affinities (see reaction (1)) obtained using different computational approaches (in kcal mol^{-1})

Molecular model[a]	Isolated complex	PCM model
H_2O	0.0	0.0
1A	161.14	19.38
1B	−111.11	−9.85
1C	−0.50	11.25
1D	17.71	44.09
1E	−40.99	−12.15
1F	−11.18	11.65
1G	−21.08	−8.47
1H[b]	−32.89	−2.34
1H[c]	−16.56	11.15
1I	−123.75	−14.90
1J	−55.90	26.05
1K	−17.24	6.24
1L	−6.29	2.79
1M	−26.71	12.46
1N	−14.87	8.46

[a] As in Fig. 1. [b] Binding through the oxygen atom. [c] Binding through the nitrogen atom.

of the solvent fails to properly describe the metal–amino acid affinities. The calculations without the solvent favor the electrostatic interactions between the carboxyl group of aspartate or glutamate and Cu^{2+} and overestimate the affinity value. Those calculations also suggest that almost all amino acids have higher affinities towards copper(II) than water and are thus able to form stable complexes with this ion. The only two exceptions are arginine, for which the DFT method predicts a highly unstable system due to an unfavorable interaction between the two positively charged species, and cystine.

To include the solvent effects in the model, we have used the PCM approach that places the investigated molecular model of the solute inside a cavity formed by a uniform and continuous solvent whose polarizability is described by a single dielectric constant. DFT/PCM calculations allowed us to improve the results obtained using the isolated-molecule approach. In the case of the Cu^{2+}–amino acid affinities, the results obtained using the PCM model are in very good agreement with experimental data. Among all the amino acid and peptide models considered in the present study, we found that the deprotonated peptide bond has the highest affinity towards Cu(II). It should be noted, however, that the peptide bond is always in the protonated state under physiological conditions, and the deprotonation may occur only at a high pH. Histidine (modeled in this work as imidazole) has the second highest affinity towards Cu(II) and, at neutral conditions, forms the most stable copper complex. Three other groups also have relatively high Cu affinity: these are the carboxyl group (which is a model of either glutamate or aspartate), the CH_3-CO-NH_2 group (a model of either glutamine, asparagine, or a peptide bond), and the NH_2-CH_3 group (a model of lysine or an N-terminus of a protein). Models of all other amino acids yield Cu affinity values lower than those for water, which suggests that in the aqueous environment Cu^{2+} can form stable complexes only with Asn, Asp, Gln, Glu, His, and Lys. This result is also in good agreement with the experimental results.[44]

To find out whether the affinity values are additive, we have considered additional model reactions:

$$[Cu(H_2O)_3(aa)]^{2+} + aa \rightarrow [Cu(H_2O)_2(aa)_2]^{2+} + H_2O \quad (2)$$

$$[Cu(H_2O)_2(aa)_2]^{2+} + aa \rightarrow [Cu(H_2O)(aa)_3]^{2+} + H_2O \quad (3)$$

$$[Cu(H_2O)(aa)_3]^{2+} + aa \rightarrow [Cu(aa)_4]^{2+} + H_2O \quad (4)$$

for some selected amino acid models. Reactions (1)–(4) allow us not only to determine the primary affinity (from reaction (1)) but also additional affinities (from reactions (2)–(4)), which we call the second, third, and fourth affinities. If the values of all four affinities are equal they are additive; this should be the case for small ligands. On the other hand, large ligands may have substantially different primary and secondary affinities. This may arise due to either sterical hindrances (leading to lower affinities) or due to the formation of intermolecular hydrogen bonds (leading to higher affinities). To analyze this effect we have calculated all the primary and secondary affinities for two systems, the histidine and serine/threonine models, and the results of the calculations are shown in Table 2.

The results demonstrate that the energy of replacing the first water molecule with an imidazole molecule to form $[Cu(H_2O)_3(imidazole)]^{2+}$ is, according to the PCM calculations, equal to −12.15 kcal mol^{-1}. The gain in energy of replacing the second water molecule to form $[Cu(H_2O)_2(imidazole)_2]^{2+}$ is −11.27, and to replace the third (to form $[Cu(H_2O)(imidazole)_3]^{2+}$) the energy gain is −9.38 kcal mol^{-1}. The energy of replacing the last water molecule to form $[Cu(imidazole)_4]^{2+}$ is only −7.80 kcal mol^{-1}. These results show that the affinity values decrease, which can be attributed to sterical hindrances and the inability of all four histidine molecules to attain the most optimal conformation in the complex corresponding to maximal interaction.

Surprisingly, a similar trend was found in the case of the serine model. For this complex the first affinity value, which leads to formation of $[Cu(H_2O)_3(serine)]^{2+}$ is equal to +2.79 kcal mol^{-1}. The addition of a second serine molecule to form $[Cu(H_2O)_2(serine)_2]^{2+}$ is more endothermic by 1.08 kcal mol^{-1}. The value of the third affinity corresponding to the formation of $[Cu(H_2O)(serine)_3]^{2+}$ is equal to

Table 2 Theoretical values of relative Cu^{2+}–amino acid affinities (see reactions (1)–(4)) obtained using different computational approaches (in kcal mol^{-1})

Affinity	Isolated complex	PCM model
H_2O	0.0	0.0
Model 1E[a]		
1st affinity	−40.99	−12.15
2nd affinity	−33.44	−11.27
3rd affinity	−27.40	−9.38
4th affinity	−23.26	−7.80
Model 1L[a]		
1st affinity	−6.29	2.79
2nd affinity	−5.53	3.87
3rd affinity	−5.05	3.34
4th affinity	−4.92	4.08

[a] As in Fig. 1.

+3.34 kcal mol^{-1}, while the last one (to form [Cu(serine)$_4$]$^{2+}$ is +4.08 kcal mol^{-1}. In this last case, however, unfavorable interactions between the serine molecules represented in the calculations by simplified models should not be a factor.

Cu^{2+}–peptide affinity

The results obtained in the first section of this work allowed us to quantify the Cu^{2+}–amino acid affinities, albeit using very simple molecular models. These models take into account the most important structural features of the amino acids crucial to the interactions between peptides or proteins and metal ions, but are lacking in some other aspects. In a peptide or a protein, the amino acids are not allowed to move freely and independently of each other since there are constraints resulting from a common backbone. These constraints may prevent some of the amino acids from attaining the most optimal configuration in interacting with the metal ion, thus effectively lowering the affinity of the system towards the ion.

To elucidate this effect, we took the His-Val-His tripeptide and calculated its interaction with Cu^{2+} in an aqueous environment. The His-Val-His tripeptide is an important system since it occurs in active centers of several enzymes, *e.g.* superoxide dismutase[54] and lysyl oxidase,[55] where it complexes copper ions. Because of this, there is much experimental evidence concerning the formation of stable 1 : 1 complexes of this system with Cu^{2+}.[33]

In this part of the work we have constructed eight molecular models representing different binding interactions of the Cu^{2+} ion with the His-Val-His peptide, depicted in Fig. 2. Models 2A and 2B represent bidentate binding of copper(II) by a -NH$_2$ group, by an imidazole moiety or by a carboxyl group, and by two water molecules. Models 2C and 2D involve a tridentate Cu^{2+} binding through one -NH$_2$ group, an imidazole group, a second imidazole or a carboxyl group, and one water molecule. Finally, systems 2E and 2G are models of tetradentate binding of a copper ion by two peptide bonds, by an imidazole, and by either a second imidazole or a carboxyl group. In this case, however, the imidazolic nitrogen of the N-terminus histidine may be either protonated or unprotonated,[56–58] which results in two additional models, 2F and 2H, respectively.

Results of this part of the study, presented in Table 3, allow us to gain insight into the geometrical features of the peptide–copper bonding. As suspected, the relative affinity of copper ions in models 2A and 2B is low due to the fact that only two water molecules are replaced by ligands with higher affinities. The same argument may be applied to models 2C and 2D in which three water molecules of the first coordination sphere of Cu^{2+} are replaced by other ligands. Here, however, a different effect may also come to play. In these two systems the peptide has to adopt a specific, not energetically favorable conformation to coordinate a copper ion, which imposes constraints and effectively lowers the affinity value.

The four other models (2E, 2F, 2G, 2H) are predicted to have high affinities towards copper ions. All four systems adopt an almost perfectly square-planar conformation around the copper ion. Additionally, the Cu^{2+} ion is chelated in all four systems by deprotonated peptide bonds, which in the previous section were predicted to have high metal affinities.

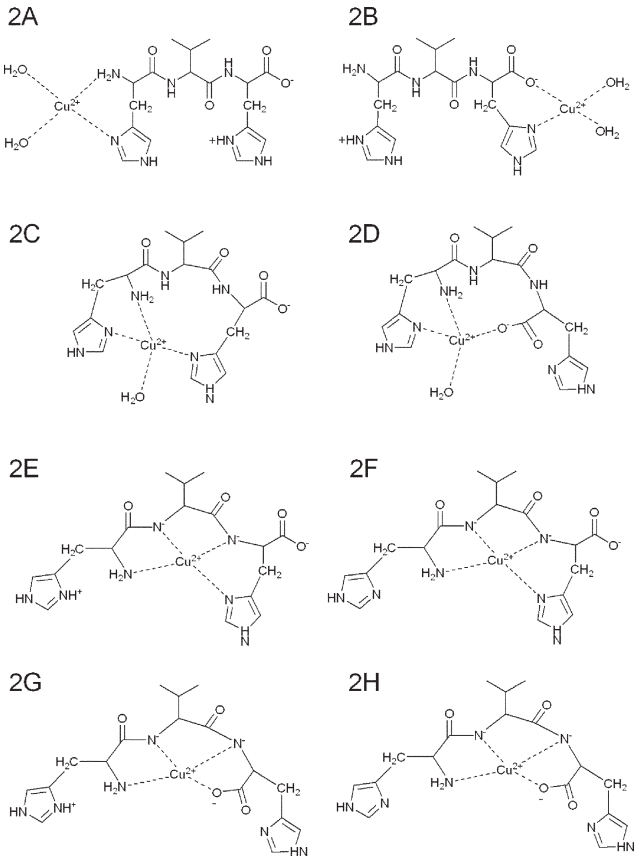

Fig. 2 Eight different modes of Cu^{2+} binding by His-Val-His tripeptide.

Table 3 Theoretical values of relative Cu^{2+}–[His-Val-His] affinities obtained using different computational approaches (in kcal mol^{-1})

Molecular model[a]	Isolated complex	PCM model
H_2O	0.0	0.0
2A	−91.72	−25.97
2B	−246.74	−32.63
2C	−76.01	−13.32
2D	−211.95	−5.13
2E	−224.58	−100.42
2F	−434.56	−97.72
2G	−12.40	−99.84
2H	−583.10	−107.43

[a] As in Fig. 2.

There is also another feature responsible for the high copper affinities in 2E, 2F, 2G, and 2H. In the presence of copper ions, the conformations of these systems are stabilized by electrostatic interaction between the ion and the peptide bonds. However, if no divalent ions are present in the solution, the two deprotonated peptide bonds located next to each other form an unfavorable arrangement leading to higher energy.

Cu^{2+}–protein affinity

The goal of the final part of this study has been to explain the selective metallization of the inner side of MTs. Since the size of the MT system is very large (~1 000 000 atoms) and the size of a single tubulin dimer is still relatively large (~13 200 atoms), DFT calculations on the whole system

 This journal is © The Royal Society of Chemistry 2006

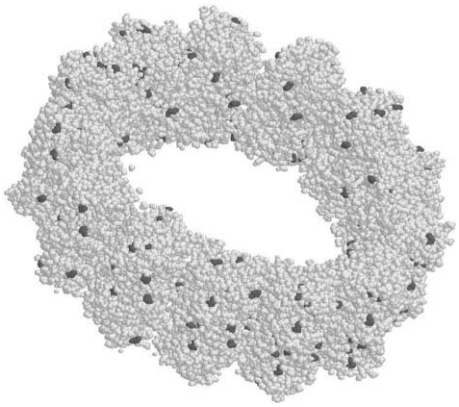

Fig. 3 A model of one MT ring consisting of 13 tubulin dimers. Dark grey colour denotes histidine residues.

would be impossible with current computers. In view of this, we had to rely on the results obtained in the calculations on both the Cu^{2+}–amino acid and Cu^{2+}–peptide systems and combine them with additional calculations on selected fragments of MTs to describe the inner MT metallization.

Our results presented in the two previous sections suggest that histidine moieties most effectively bind Cu^{2+} ions. A tubulin dimer consists of 877 amino acid residues, but among them there are only 23 histidine residues, mostly located on the surface of the protein.[20,21] For a single dimer they all are good candidates to bind copper(II) ions. However, when an MT is formed, some of the histidines become buried inside the MT structure. A visual analysis of the MT model[19] presented in Fig. 3 reveals that there are 11 histidine moieties in every tubulin dimer of MT, which have at least a part of the imidazole ring exposed to the solution. Five of them are located on the inner surface of the MT; these are 28A, 61A, 283A, 37B, and 229B (with names according to the naming of 1JFF model in the PDB database).[20] The remaining six—309A, 393A, 406A, 192B, 309B, and 406B—are located on the outer surface of the MT (see Fig. 4).

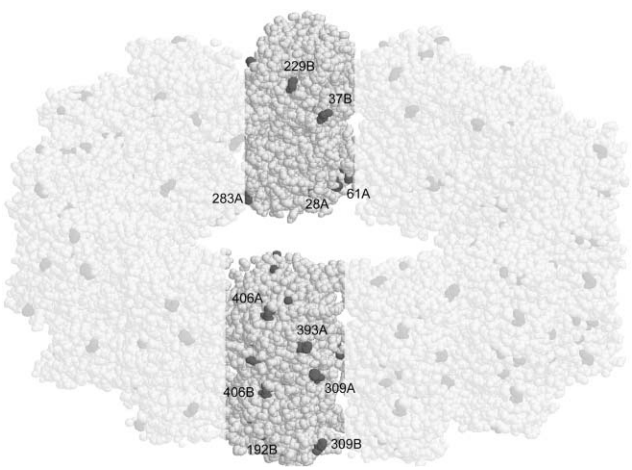

Fig. 4 Visualization of surface histidines (dark grey) exposed to the solution. There are five inner-surface histidines (28A, 61A, 283A, 37B, 229B) and six outer-side histidines (309A, 393A, 406A, 192B, 309B, 406B).

After selecting 11 possible metallization sites, the following procedure was used to create molecular models for describing the histidine metallization:

- select all amino acids within 3.0 Å of the histidines to yield moderate size models;
- replace amino acid side-chains located relatively far from the histidine moiety by hydrogens;
- add all other missing hydrogen atoms and optimize their positions using the molecular mechanics method with the amber96 force-field;
- optimize the geometry of the whole system using the same method, with the positions of the backbone atoms kept frozen; and,
- perform additional geometry optimization using the semiempirical PM3 method, with the positions of the backbone atoms kept frozen.

This procedure yielded 11 molecular models of possible metallization sites, ranging from 40 to 70 atoms in size. Next, a Cu^{2+} ion and additional water molecules were added to each model to complete the coordination sphere around the copper ion (see Fig. 5 and 6). In the next step, the structures of all the

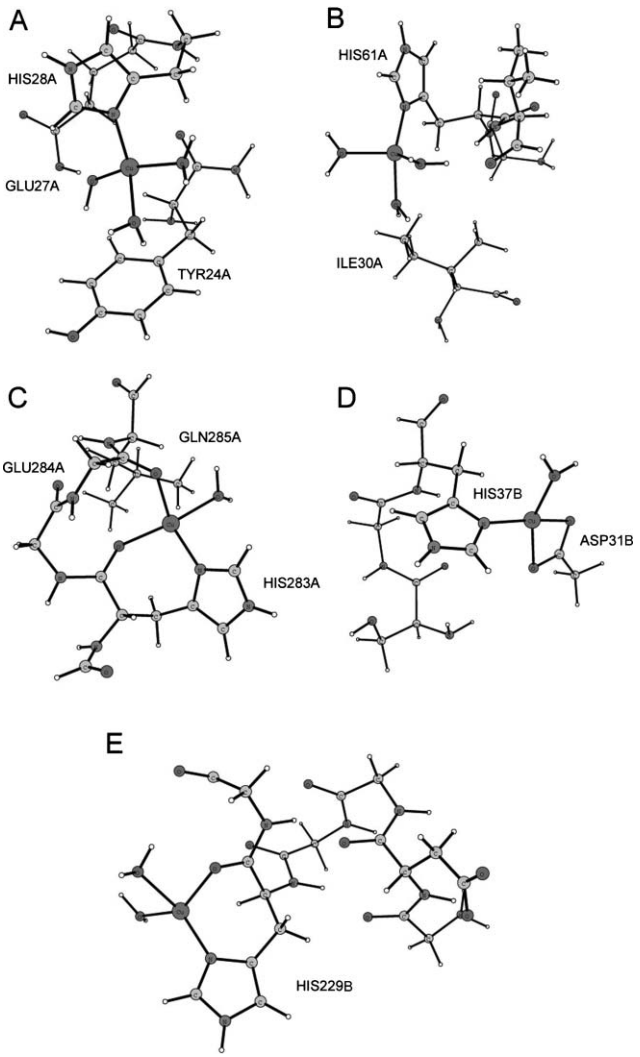

Fig. 5 Molecular models of the five inner-surface metallization sites complexing Cu^{2+}: A 28A, B 61A, C 283A, D 37B, E 229B.

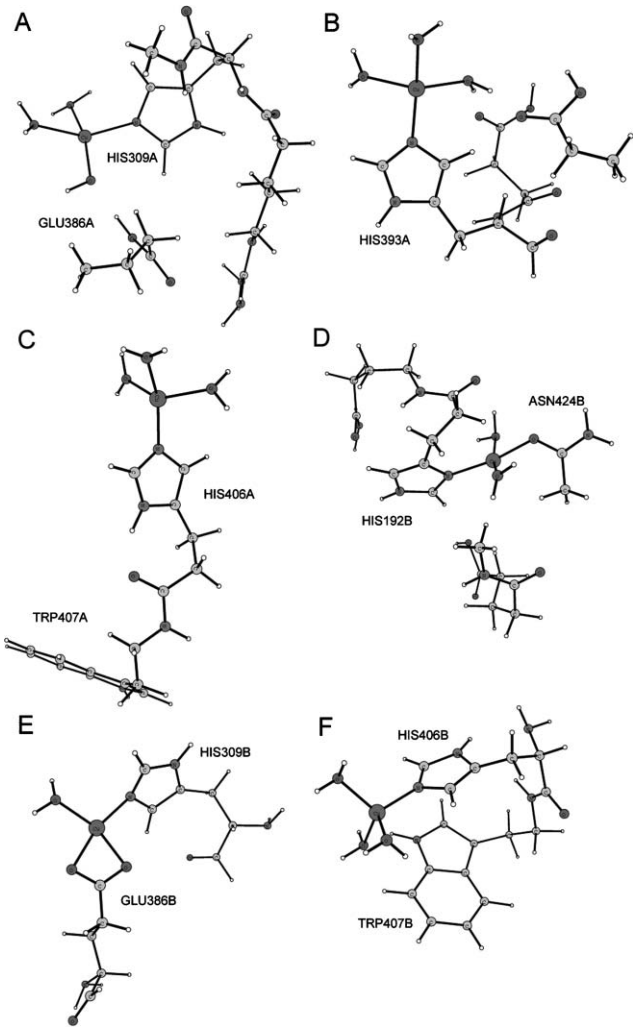

Fig. 6 Molecular models of the six outer-surface metallization sites complexing Cu^{2+}: A 309A, B 393A, C 406A, D -192B, E 309B, F 406B.

models were optimized using the DFT/B3LYP method and the copper affinities were determined for the models using the same procedure as for the Cu^{2+}–amino acid and the Cu^{2+}–peptide systems.

The equilibrium DFT/B3LYP geometries of the models allowed us to analyze some geometrical features of all 11 metallization sites. Using the results described in the previous sections of this work, each metallization site was divided into fragments with known affinities towards copper(II) (see Table 4). The results of this analysis show that five of the 11 metallization sites (28A, 61A, 393A, 406A, 406B) do not have any relevant amino acid side chains in the vicinity of the imidazole. In those metallization sites, the Cu^{2+} ion is complexed by only one imidazole moiety and by three water molecules. The geometrical analysis suggests, in these cases, a low affinity value. Four other metallization sites (283A, 309A, 229B, 192B) allow for Cu^{2+} complexation by both the imidazole moiety and the $CO\text{-}CH_3\text{-}NH_2$ moiety. These sites should have higher affinity values according to the results obtained in the first section of this work (see Table 1). The last two metallization sites (37B, 309B) have structures involving an imidazole moiety positioned close to a carboxyl group, which should also yield strong Cu^{2+} binding.

Table 4 Theoretical values of relative Cu^{2+}–tubulin fragments affinities obtained using different computational approaches (in kcal mol^{-1})

Molecular model[a]	Geometry[b]	Isolated complex	PCM model
H_2O	—	0.0	0.0
Inner surface of MT			
28A	$1E + 3H_2O$	—	—
61A	$1E + 3H_2O$	—	—
283A	$1E + 1H + 2H_2O$	−97.65	−150.22
37B	$1E + 1B + 1H_2O$	−237.57	−187.94
229B	$1E + 1H + 2H_2O$	−189.61	−151.12
Outer surface of MT			
309A	$1E + 1H + 2H_2O$	−151.61	−152.53
292A	$1E + 3H_2O$	—	—
406A	$1E + 3H_2O$	—	—
192B	$1E + 1H + 2H_2O$	−93.09	−150.19
309B	$1E + 1B + 1H_2O$	−217.30	−172.07
406B	$1E + 3H_2O$	—	—

[a] As in Fig. 4. [b] The amino acid fragments (as in Fig. 1) in the first coordination sphere of Cu^{2+} ion.

A simple analysis of the geometrical features of the 11 model structures suggests that the two best candidates for metallization sites within the tubulin dimer are histidine moieties 37B (located on the inner surface of MT) and 309B (on the outer surface of MT). Such an analysis is, however, somewhat inaccurate since it does not take into account the interactions between the chemical groups complexing the Cu^{2+} ion and the rigidity of the protein backbone. To obtain more precise absolute and relative affinity values, a set of the six potentially most effective metallization sites was selected, and a computational approach described earlier was used to calculate their affinities towards the copper ion.

Four of the six selected sites (283A, 309A, 192B, 229B) with Cu^{2+} chelated by a histidine residue, a peptide bond, and two water molecules have similarly low affinities. As expected, the two other sites (37B, 309B), where Cu^{2+} is chelated by a histidine residue, a glutamate or aspartate residue, and one water molecule, have much higher affinities than the 283A, 309A, 192B, and 229B sites. At the same time the affinity of the 37B site is much higher than the affinity of the 309B site. In the former system the backbone of the protein allows the chelating groups to adopt the most optimal conformation around the copper ion. For the latter site, the conformation of the chelating groups is far from optimal due to structural constraints and this results is a lower affinity.

Conclusions

The metallization of the inner surface of microtubules may become a powerful technique in constructing nanoscale interconnectors and possibly other nanoelectronic devices. To explain the selectivity of the metallization process we have performed DFT computational studies of the Cu^{2+} binding to different molecular fragments of MTs. The results provided a detailed description of the energetic and geometrical features of the biocomplexes formed by copper ions. The results of this work also provide an explanation of why electroless plating of

 This journal is © The Royal Society of Chemistry 2006

microtubules by copper leads to inner-tube copper deposition. In the search for this explanation, we have identified 11 molecular sites within a tubulin dimer that are good candidates for the metallization sites. Based on simple amino acid analysis of the sites, we have chosen five sites with expected high affinities towards Cu^{2+} ions. The results of the calculations suggest that site 37B, found on the inner side of the MT, has the highest affinity towards copper ions and is, therefore, the most probable target for the metallization. Moreover, this site has another advantage over the metallization sites located on the outer surface of the MT. In general, the number of metallization sites per tubulin dimer on the inner side of the MT is nearly equal to the number of sites on the outer side, but their density per unit volume is higher due to the smaller surface of the inner MT side in comparison to the outer side. It must be noted, however, that the uptake of copper ions by the inner side of the MT should not be attributed only to the high affinities toward copper ions of individual metallization sites. There are other factors that may affect this process, with diffusion likely being the most important one. Unfortunately, these phenomena cannot be described by the approach used in this work.

Additionally, this study provided a systematic theoretical investigation of the affinities of various Cu^{2+}–amino acid systems and the equilibrium structures of these systems. In future work, the investigation will be extended to other metal ions, as well as other fragments of biosystems (*i.e.* fragments of DNA or RNA). Theoretical calculations of this kind have frequently been a useful prerequisite to experimentation. This includes experiments concerning development of the metallization technology at the nano scale. The computational approach proposed in this work may become a useful tool for predicting the metallization sites for not only copper but also other metals and other biomolecules. A relatively fast, yet accurate, computational approach may guide experimental efforts concerning metallization by predicting possible best metallization sites and their affinities towards different metals.

Acknowledgements

NSF grant #0303863 and CPU time from University of Arizona supercomputing center are gratefully acknowledged. Fig. 1, 5, and 6 were generated using the xyzviewer software designed by Sven de Marothy. Fig. 3 and 4 were generated using Rasmol software.[59]

References

1 Y. Huang, X. Duan, Q. Wei and C. M. Lieber, *Science*, 2001, **291**, 630.
2 R. F. Service, *Science*, 2001, **293**, 782.
3 G. Y. Tseng and J. C. Ellenbogen, *Science*, 2001, **292**, 1293.
4 J. H. Schön, H. Meng and Z. Bao, *Nature*, 2001, **413**, 713.
5 E. Braun, Y. Eichen, U. Sivan and G. Ben-Yoseph, *Nature*, 1998, **391**, 775.
6 J. Richter, R. Seidel, R. Kirsch, M. Mertig, W. Pompe, J. Plaschke and H. K. Schackert, *Adv. Mater.*, 2000, **12**, 507.
7 Z. Deng and C. Mao, *Nano Lett.*, 2003, **3**, 1545.
8 W. E. Ford, O. Harnack, A. Yasuda and J. M. Wessels, *Adv. Mater.*, 2000, **12**, 1793.
9 M. Mertig, L. C. Ciacchi, R. Seidel and W. Pompe, *Nano Lett.*, 2002, **2**, 841.
10 K. Keren, M. Krueger, R. Giland, G. Ben-Yoseph, U. Sivan and E. Braun, *Science*, 2002, **297**, 72.
11 K. Keren, R. S. Berman and E. Braun, *Nano Lett.*, 2004, **4**, 323.
12 C. F. Monson and A. T. Wooley, *Nano Lett.*, 2003, **3**, 359.
13 H. A. Becerill, R. M. Stoltenberg, C. F. Monson and A. T. Wooley, *J. Mater. Chem.*, 2004, **14**, 611.
14 Q. Gu, C. Cheng and D. T. Haynie, *Nanotechnology*, 2005, **16**, 1358.
15 M. Knez, A. M. Bittner, F. Boes, C. Wege, H. Jeske, E. Maiß and K. Kern, *Nano Lett.*, 2003, **3**, 1079.
16 M. Knez, M. Sumser, A. M. Bittner, C. Wege, H. Jeske, T. Martin and K. Kern, *Adv. Funct. Mater.*, 2004, **14**, 116.
17 R. R. Naik, S. E. Jones, C. J. Murray, J. C. McAuliffe, R. A. Vaia and M. O. Stone, *Adv. Funct. Mater.*, 2004, **14**, 25.
18 I. A. Banerjee, L. Yu and H. Matsui, *Proc. Natl. Acad. Sci. U. S. A.*, 2003, **100**, 14678.
19 E. Nogales, M. Whittaker, R. A. Milligan and K. H. Downing, *Cell*, 1999, **96**, 77.
20 E. Nogales, S. G. Wolf and K. H. Downing, *Nature*, 1998, **391**, 199.
21 J. Lowe, H. Li, K. H. Downing and E. Nogales, *J. Mol. Biol.*, 2001, **313**, 1045.
22 S. Schulyer and D. Pellman, *Cell*, 2001, **105**, 421.
23 H. Lodish, A. Berk, L. S. Zipursky, P. Matsuidara, D. Baltimore and J. Darnell, *Molecular Cell Biology*, W. H. Freeman & Co., New York, 2000.
24 Y. Yang, P. Deymier, L. Wang, R. Guzman, J. B. Hoying, H. J. McLaughlin, S. D. Smith and I. N. Jongewaard, *Biotechnol. Prog.*, 2006, **22**, 303.
25 Y. Yang, R. Guzman, P. A. Deymier, M. Umnov, J. B. Hoying, S. Raghavan, O. Palusinski and B. J. J. Zelinski, *J. Nanosci. Nanotechnol.*, 2005, **5**, 2050.
26 B. Trzaskowski, F. Leonarski, A. Leś and L. Adamowicz, *J. Phys. Chem. B*, 2005, **109**, 17734.
27 M. Mertig, R. Kirsch and W. Pompe, *Appl. Phys. A*, 1008, **66**, s723.
28 Y. Yang, B. H. Constance, P. A. Deymier, J. Hoying, S. Raghavan and B. J. J. Zelinski, *J. Mater. Sci.*, 2004, **39**, 1927.
29 K. Valenzuela, S. Raghavan, P. A. Deymier and J. Hoying, upublished work.
30 P. E. M. Siegbahn and M. R. A. Blomberg, *Annu. Rev. Phys. Chem.*, 1999, **50**, 221.
31 P. E. M. Siegbahn, *Theor. Chem. Acc.*, 2001, **105**, 197.
32 C. W. Bauschlicher, Jr. and P. Maitre, *J. Chem. Phys.*, 1995, **99**, 3444.
33 A. Myari, G. Malandrinos, Y. Deligiannakis, J. C. Plakatouras, N. Hadjiladis, Z. Nagy and I. Sòvágó, *J. Inorg. Biochem.*, 2001, **85**, 253.
34 P. E. M. Siegbahn and M. R. A. Blomberg, *Chem. Rev.*, 2000, **100**, 421.
35 A. Becke, *J. Chem. Phys.*, 1993, **98**, 5648.
36 C. Lee, W. Yang and R. Parr, *Phys. Rev. B*, 1988, **37**, 785.
37 W. D. Cornell, P. Cieplak, C. I. Bayly, I. R. Gould, K. M. Mertz, jr., D. M. Ferguson, D. C. Spellmeyer, T. Fox, J. W. Caldwell and P. A. Kollman, *J. Am. Chem. Soc.*, 1995, **117**, 5179.
38 J. J. P. Stewart, *J. Comput. Chem.*, 1989, **10**, 209.
39 S. Miertus, E. Scrocco and J. Tomasi, *Chem. Phys.*, 1981, **55**, 117.
40 F. Himo and P. E. M. Siegbahn, *Chem. Rev.*, 2003, **103**, 2421.
41 NIST Computational Chemistry Comparison and Benchmark Database, NIST Standard Reference Database Number 101, Release 12, August 2005, ed. R. D. Johnson III.
42 M. J. Frisch, G. W. Trucks, H. B. Schlegel, G. E. Scuseria, M. A. Robb, J. R. Cheeseman, J. A. Montgomery, Jr., T. Vreven, K. N. Kudin, J. C. Burant, J. M. Millam, S. S. Iyengar, J. Tomasi, V. Barone, B. Mennucci, M. Cossi, G. Scalmani, N. Rega, G. A. Petersson, H. Nakatsuji, M. Hada, M. Ehara, K. Toyota, R. Fukuda, J. Hasegawa, M. Ishida, T. Nakajima, Y. Honda, O. Kitao, H. Nakai, M. Klene, X. Li, J. E. Knox, H. P. Hratchian, J. B. Cross, V. Bakken, C. Adamo, J. Jaramillo, R. Gomperts, R. E. Stratmann, O. Yazyev, A. J. Austin, R. Cammi, C. Pomelli, J. Ochterski, P. Y. Ayala, K. Morokuma, G. A. Voth, P. Salvador, J. J. Dannenberg, V. G. Zakrzewski, S. Dapprich, A. D. Daniels, M. C. Strain, O. Farkas, D. K. Malick, A. D. Rabuck, K. Raghavachari, J. B. Foresman, J. V. Ortiz, Q. Cui, A. G. Baboul, S. Clifford, J. Cioslowski, B. B. Stefanov, G. Liu,

A. Liashenko, P. Piskorz, I. Komaromi, R. L. Martin, D. J. Fox, T. Keith, M. A. Al-Laham, C. Y. Peng, A. Nanayakkara, M. Challacombe, P. M. W. Gill, B. G. Johnson, W. Chen, M. W. Wong, C. Gonzalez and J. A. Pople, *GAUSSIAN 03 (Revision C.02)*, Gaussian, Inc., Wallingford, CT, 2004.
43 U. Weser, E. Bunnenberg, R. Camack, C. Djerassi, L. Flohé, G. Thomas and W. Voelter, *Biochim. Biophys. Acta*, 1971, **243**, 203.
44 W. Voelter, G. Sokolowski, U. Weber and U. Weser, *Eur. J. Biochem.*, 1975, **58**, 159.
45 J. M. McCord and I. Fridovich, *J. Biol. Chem.*, 1968, **243**, 5753.
46 J. M. McCord and I. Fridovich, *J. Biol. Chem.*, 1969, **244**, 6049.
47 H. Siegel and R. B. Martin, *Chem. Rev.*, 1982, **82**, 385.
48 M. Romanelli and R. Basosi, *Chem. Phys. Lett.*, 1988, **143**, 404.
49 K. Takebara and Y. Ide, *Inorg. Chim. Acta*, 1991, **186**, 73.
50 S. Materazzi, R. Curini and G. D'Ascenzo, *Thermochim. Acta*, 1996, **275**, 93.
51 P. Manikandan, B. Epel and D. Goldfarb, *Inorg. Chem.*, 2001, **40**, 781.
52 F. Carrera, E. Sánchez Marcos, P. J. Merkling, J. Chaboy and A. Muñoz-Páez, *Inorg. Chem.*, 2004, **43**, 6674.
53 H. Kozłowski, T. Kowalik-Jankowska and M. Jeżowska-Bojczuk, *Coord. Chem. Rev.*, 2005, **249**, 2323.
54 J. A. Tainer, E. D. Getzoff, K. M. Beem, J. S. Richardson and D. C. Richardson, *J. Mol. Biol.*, 1982, **160**, 181.
55 H. M. Kagan and W. Li, *J. Cell. Biochem.*, 2003, **88**, 660.
56 I. Sòvágó, E. Farkas and A Gergely, *J. Chem. Soc., Dalton Trans.*, 1982, 2159.
57 E. Farkas, I. Sòvágó, T. Kiss and A. Gergely, *J. Chem. Soc., Dalton Trans.*, 1984, 611.
58 C. E. Livera, L. D. Petit, M. Bataille, B. Perly, H. Kozłowski and B. Radomska, *J. Chem. Soc., Dalton Trans.*, 1987, 661.
59 R. Sayle and E. J. Milner-White, *Trends Biochem. Sci.*, 1995, **20**, 374.

Looking for that special chemical biology research paper?

TRY this free news service:

Chemical Biology

- highlights of newsworthy and significant advances in chemical biology from across RSC journals
- free online access
- updated daily
- free access to the original research paper from every online article
- also available as a free print supplement in selected RSC journals.*

*A separately issued print subscription is also available.

Registered Charity Number: 207890

22030681

RSC Publishing

www.rsc.org/chembiology

 This journal is © The Royal Society of Chemistry 2006